

<https://doi.org/10.1038/s43247-024-01884-9>

Frazil ice changes winter biogeochemical processes in the Lena River



Sophie Opfergelt¹✉, François Gaspard¹, Catherine Hirst^{1,2}, Laurence Monin¹, Bennet Juhls³, Anne Morgenstern³, Michael Angelopoulos³ & Pier Paul Overduin³

The ice-covered period of large Arctic rivers is shortening. To what extent will this affect biogeochemical processing of nutrients? Here we reveal, with silicon isotopes ($\delta^{30}\text{Si}$), a key winter pathway for nutrients under river ice. During colder winter phases in the Lena River catchment, conditions are met for frazil ice accumulation, which creates microzones. These are conducive to a lengthened reaction time for biogeochemical processes under ice. The heavier $\delta^{30}\text{Si}$ values (3.5 ± 0.5 ‰) in river water reflect that $39 \pm 11\%$ of the Lena River discharge went through these microzones. Freezing-driven amorphous silica precipitation concomitant to increased ammonium concentration and changes in dissolved organic carbon aromaticity in Lena River water support microbially mediated processing of nutrients in the microzones. Upon warming, suppressing loci for winter intra-river nitrogen processing is likely to modify the balance between N_2O production and consumption, a greenhouse gas with a large global warming potential.

With warming occurring four times faster in the Arctic than globally¹, the ice-covered period for large rivers is shortening², and is projected to be at least 20 days shorter on average across the Arctic by the end of this century³. In large Arctic rivers, winter is key for the sub-ice biogeochemical processing of essential nutrients such as nitrogen (N)^{4–6}, supplying this limiting nutrient to the Arctic Ocean. During winter conditions less oxygen can diffuse into the water column and bacteria rely on alternative electron acceptors to metabolize organic carbon (C). Water column dynamics of large Arctic rivers in the winter depend on river ice formation. Nitrogen cycling drives organic matter degradation under lake ice⁷ and in marine water columns^{8,9} but is generally overlooked as a driver of organic matter degradation in large Arctic rivers. To predict the consequences of shortening river ice duration on major biogeochemical cycles such as C and N that control vertical greenhouse gas release and lateral C and N fluxes, we need to constrain how river ice formation influences the reaction time for biogeochemical processes in the water column.

Here, we show that river water with temperatures below freezing (supercooling) and turbulent flow can trigger the accumulation of ice crystals below the stable ice cover. Forced to flow as interstitial water through the ice crystals, water velocity is decreased for a portion of the river discharge. This creates a more physically isolated environment where oxygen supply is more limited and prolongs the conducive condition period for microbial activity in these ice-driven microzones.

We use the dissolved silicon (Si) isotope composition ($\delta^{30}\text{Si}$) and the germanium to silicon ratio (Ge/Si) of an Arctic river during the winter to determine the influence of ice crystal formation on reaction time for solutes

in the water column. Ice formation increases the Si concentration in the interstitial water, which can lead to the supersaturation and precipitation of amorphous silica. This precipitation preferentially incorporates the lighter Si isotopes in amorphous silica, and includes Si over Ge, leaving the interstitial water with an isotopically heavier $\delta^{30}\text{Si}$ and a higher Ge/Si ratio.

For an entire year, we present a high resolution (about every 5 days) time series of Si isotope composition and Ge/Si ratio in river water samples collected at the outlet of one of the largest Arctic rivers, the Lena River (Research Station Samoylov Island; Fig. 1; see Methods for environmental setting). We integrate these observations with air temperature re-analysis data, catchment topography, discharge data, water temperature data, ice thickness measurements, and ice growth rate modelling data to determine conditions for river ice formation at high temporal resolution during winter. We support our findings with geochemical parameters to highlight the influence of additional ice formation during cold winter phases on biogeochemical processes involved in key nutrient cycles such as C and N. We demonstrate that colder winter periods can trigger microzones where solutes have a longer reaction time, which extends the window for sub-ice biogeochemical processing of nutrients.

Results and discussion

Microzones with longer reaction time for biogeochemical processes in the water column

The highest Si isotope composition (3.5 ± 0.5 ‰) and the highest Ge/Si ratio (2.2 ± 0.6 $\mu\text{mol/mol}$) in the river water are found during the

¹Earth and Life Institute, UCLouvain, Louvain-la-Neuve, Belgium. ²Earth Science Department, Durham University, Durham, United Kingdom. ³Alfred Wegener Institute Helmholtz Centre for Polar and Marine Research, Potsdam, Germany. ✉e-mail: sophie.opfergelt@uclouvain.be

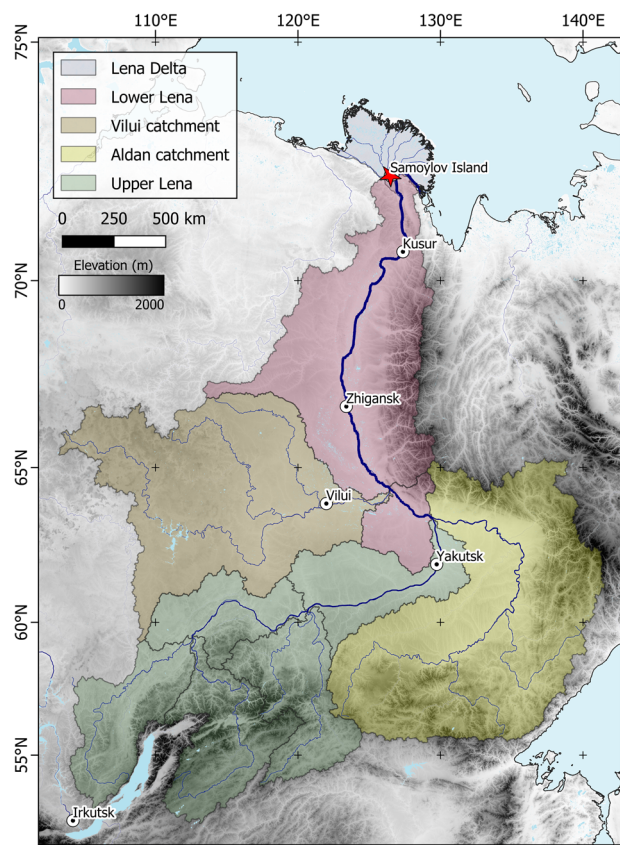


Fig. 1 | The Lena River catchment. Sampling location (Samoylov Island; red star) at the outlet of the Lena River catchment comprising four major sub-catchments, with contribution to annual streamflow for the Upper Lena (42%), the Aldan (30%), the Vilui (9%), and the Lower Lena (19%) catchments²⁰ with digital elevation model of the Lena catchment (GEBCO Grid).

ice-covered period relative to the open water period (Fig. 2a-c). The sharp increase in $\delta^{30}\text{Si}$ and Ge/Si supports that during phases of the winter, the conditions are met for amorphous silica precipitation. Freezing can increase the concentration of Si above the solubility for amorphous silica¹⁰. Evidence that amorphous silica formed during the ice-covered period is given by the dissolved Si concentration at the Lena outlet plateau at $142 \pm 5 \mu\text{M}$ between December and March, whereas the water electrical conductivity increases during the same period (Supplementary Fig. 1). With increasing river ice thickness (Fig. 3c), salt exclusion from the ice controls the increase in electrical conductivity, but the plateau in dissolved Si concentration reflects a relative Si loss from the dissolved phase into amorphous silica precipitates. The precipitation of amorphous silica upon freezing induces a kinetic Si isotope fractionation with solids formed that are up to +5 ‰ lighter in their $\delta^{30}\text{Si}$ than the corresponding solution¹¹⁻¹³. The high Ge/Si ratios support the formation of amorphous silica: Ge, which is not preferentially incorporated into amorphous silica, accumulates in solution leading to an increase in Ge/Si ratio in water¹⁴. The lag in the onset of the Ge/Si increase relative to the $\delta^{30}\text{Si}$ increase (Fig. 3d) in water with amorphous silica precipitation is well known and results from the fact that Ge incorporation rates are orders of magnitude slower than Si precipitation rates¹⁴.

To reach the solubility limit for amorphous silica precipitation within the Lena River, microzones must form where freezing leads to an increase in Si concentration. Considering the Si concentration in the Lena River water during the ice-covered period ($0.14 \pm 0.01 \text{ mM}$)¹⁵ and the solubility limit for amorphous silica precipitation (1.1 mM at 0°C)¹⁰, there is a need for a factor of 8 concentration in the river water dissolved Si to reach the solubility limit for amorphous silica precipitation. Microzones in the water column can be

generated from the accumulation of frazil ice, i.e., individual sub-mm to mm-sized ice crystals randomly oriented with various shapes. In a turbulent water flow such as the Lena River (Fig. 3b) with supercooled water (Fig. 3b), the conditions are met for frazil ice formation¹⁶. Supercooled water is evident during the first half of the winter when the Lena River water temperature at the outlet is at -0.2°C with returns to 0°C with the release of latent heat following ice formation, and during the second half of winter when the river water temperatures are -0.3°C (Fig. 3b). Support for frazil ice formation is provided by the difference in $\delta^{18}\text{O}$ in river water between the outlet of the catchment (Samoylov) and about 800 km upstream (Zhigansk)¹⁷ (see Methods; Supplementary Fig. 2). The comparison highlights that between November 2018 and February 2019, downstream water from Samoylov present heavier $\delta^{18}\text{O}$ values than upstream water from Zhigansk¹⁷. This difference in $\delta^{18}\text{O}$ in water between the two sampling locations can be used to support the formation of frazil ice and the higher presence of frazil ice crystals in the water samples from downstream (Samoylov). Indeed, oxygen isotope fractionation upon river ice formation leads to river ice being isotopically heavier relative to the respective water source, and frazil ice crystals entrained in flow can accumulate to be more abundant downstream (Fig. 4).

Once formed, the frazil ice moves with water flow and tends to accumulate at slope transitions (at pressure ridges where the river ice cover is disturbed, or at transition from steep to shallow slopes¹⁸) or sticks to bed matter to form anchor ice¹⁹ (Fig. 4). By adding up the contribution to flow discharge from the Upper Lena (42%), the Aldan (30%) and the Lower Lena (19%)²⁰, more than 90% of the Lena streamflow originates from sub-catchments with marked slope transitions from mountainous areas (e.g., the Trans Baikal Highlands and Verkhoyansk Mountain Range) to narrower lowlying areas adjacent to the main channel (Fig. 1b), with the remaining discharge derived from the lowlying Central Siberian Plateau. The accumulation of frazil ice forms an agglomerate of ice crystals not cemented containing interstitial water (Fig. 4). The hydraulic conductivity, i.e. a property of porous materials that describes the ease with which a fluid such as water can move through the pore space, of a frazil agglomerate is on the order of those for fine sand²¹. This sets a difference in flow speed in frazil agglomerates orders of magnitude lower than the rest of the water column. This increases reaction time for solutes in frazil agglomerates at different times at different locations in the entire catchment without modifying the total river discharge. The Si concentration in interstitial waters within frazil agglomerates can increase upon further freezing, frazil ice crystal formation and Si expulsion together with a rise in electrical conductivity²². Upon amorphous silica precipitation, the associated Si isotope fractionation leads to heavier Si isotope composition in the interstitial water. The interstitial water moves through the frazil agglomerate and mixes with river water (Fig. 4).

Conditions for frazil ice formation are intensified during colder winter phases (air temperature $< -30^\circ\text{C}$), leading to optimal conditions for amorphous silica precipitation. This explains why the first cold phase is associated with an increase in $\delta^{30}\text{Si}$ in water (Fig. 3a,d). This corresponds to the early winter when the river ice thickness is still below 50 cm (Fig. 3c). In contrast, during the second half of the winter, there is a lag time between the decrease in air temperature and the heavy $\delta^{30}\text{Si}$ values (Fig. 3a,d) explained by the thicker river ice (above 80 cm; Fig. 3c) raising the transfer time for changes in air temperature to impact below ice²³ and delaying the amorphous silica precipitation. This hypothesis is supported by the modeled ice growth rate, which is lower during the second half of the winter relative to the first half (Fig. 3c).

At the end of the winter before the ice break-up, the air temperature rises first at lower latitudes in the Lena catchment (Supplementary Fig. 3). Upon a rise in water temperature before the ice break-up¹⁵, frazil ice thaws and releases interstitial water from the microzones. This leads to an increase in water electrical conductivity at the Lena River outlet driven by the release of accumulated salt¹⁵, but also to a decrease in dissolved Si concentration¹⁵ (Supplementary Fig. 1) and a heavy $\delta^{30}\text{Si}$ value in river water just before ice break-up (Fig. 2c). These data support the hypothesis of Si loss by

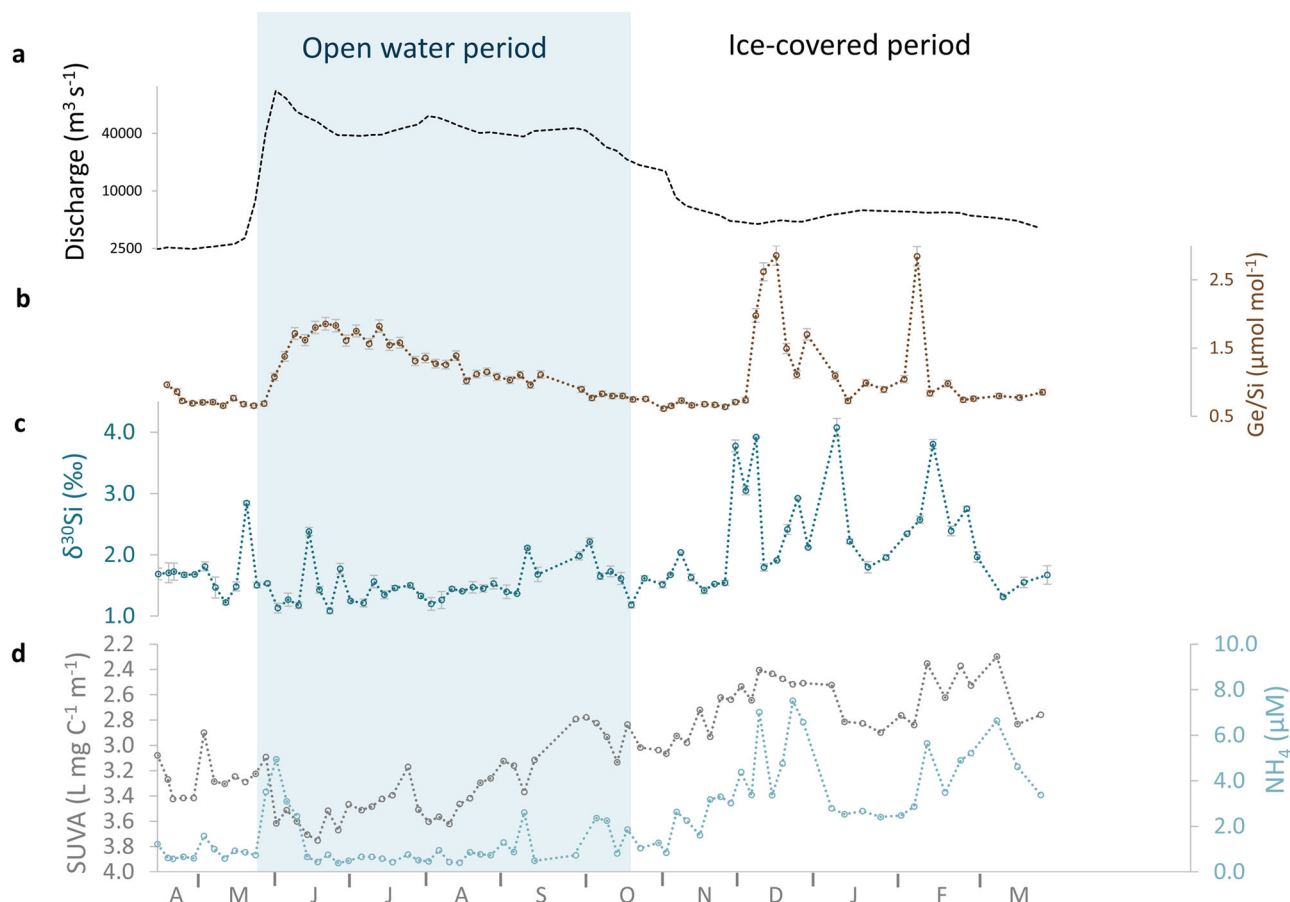


Fig. 2 | One-year chemical monitoring of the Lena River water. Between 20th April 2018 and 28th March 2019 (A, M, J, J, A, S, O, N, D, J, F, M: months from April until March) at Samoylov station including the open water period (blue area) and the ice-

covered period: (a) Discharge close to Samoylov station for the Lena catchment (Roshydromet¹²); (b) Ge/Si ratio (\pm SD); (c) Si isotope composition (\pm SD); (d) SUVA values (Y-axis reverted) and dissolved NH_4 concentrations¹⁵.

precipitation of amorphous silica in microzones during the winter, with no redissolution of amorphous silica into water at ice break-up.

Influence of river ice on winter microbially mediated biogeochemical processes in the water column

Using Si isotope and Ge/Si data, we demonstrate that microzones exist within river ice and increase the reaction time for solutes in the water column of the Lena River during winter months. The Si isotope composition measured at the Lena outlet during the ice-covered period can be used to estimate the portion of the Lena River water flowing through these microzones. According to an isotope mass balance calculation (see Methods; Supplementary Fig. 4), before reaching the outlet of the Lena catchment at Samoylov station, $39 \pm 11\%$ of the total discharge of the Lena River went through microzones triggered by cold phases during the winter 2018–2019 (heavier $\delta^{30}\text{Si}$ values on 28/11/18, 02/12/18, 06/12/18, 22/12/18, 06/01/19, 12/02/19, 25/02/19), whereas $7 \pm 7\%$ of the Lena River discharge went through microzones during the rest of the ice-covered period of that winter (24/10/18 to 28/03/19). This underlines the importance of these microzones at the catchment scale. Here we propose that these microzones meet the conditions for microbially mediated biogeochemical processes. The microzones in river ice are analogous to the microzone development in the hyporheic zone, i.e., the porous sediment area beneath stream bed²⁴. In both situations, interstitial waters are isolated from renewed oxygen supply leading to a decrease in oxygen concentration and prompting bacteria to use alternative electron acceptors for the degradation of riverine dissolved organic matter, e.g., nitrate for denitrifying bacteria²⁴. We provide evidence that microzones are loci for nitrogen cycling in the Lena River during winter months: we

observe higher concentrations of ammonium (NH_4), the most reduced form of dissolved inorganic nitrogen, during the ice-covered period relative to the open water period (Fig. 2d). Notably the increase in NH_4 concentration in the winter directly follows a cold phase when the river ice cover is thin (early winter) and appears with a lag time after a cold phase when the river ice is thicker (late winter) (Fig. 3e). These data suggest microbially driven NH_4 enrichment, either from nitrate reduction or from organic N mineralisation, occurring below ice during the winter in microzones. Support for qualitative changes in dissolved organic matter is provided by a concomitant shift to lower specific ultraviolet absorbance (SUVA) values reflecting a change towards less aromatic dissolved organic carbon (Fig. 3e). The elevated NH_4 and low SUVA values in under-ice river waters provide evidence for microbially mediated biogeochemical processing of C and N in microzones, considering that external C and N inputs to the water column from hyporheic zones and groundwater flow paths are limited during the winter²⁵. This confirms that micro-niche conditions control microbial activity involved in key nutrients cycles such as C and N during winter times²⁶.

The formation of microzones for microbially driven biogeochemical processes during river ice formation depends on the two conditions for frazil ice formation: turbulent flow and supercooled water. The higher the flow discharge, the more turbulent the flow below ice²⁷. Data from monitoring at Samoylov station across four winters between 2018 and 2022²⁸ showcase the effect of different conditions on biogeochemical processing. (i) None of the conditions of turbulent flow and supercooled water temperature are met in winters 2019–2020 and 2020–2021 (i.e., discharge is low and water temperature is $>$ or at -0.1°C (Supplementary

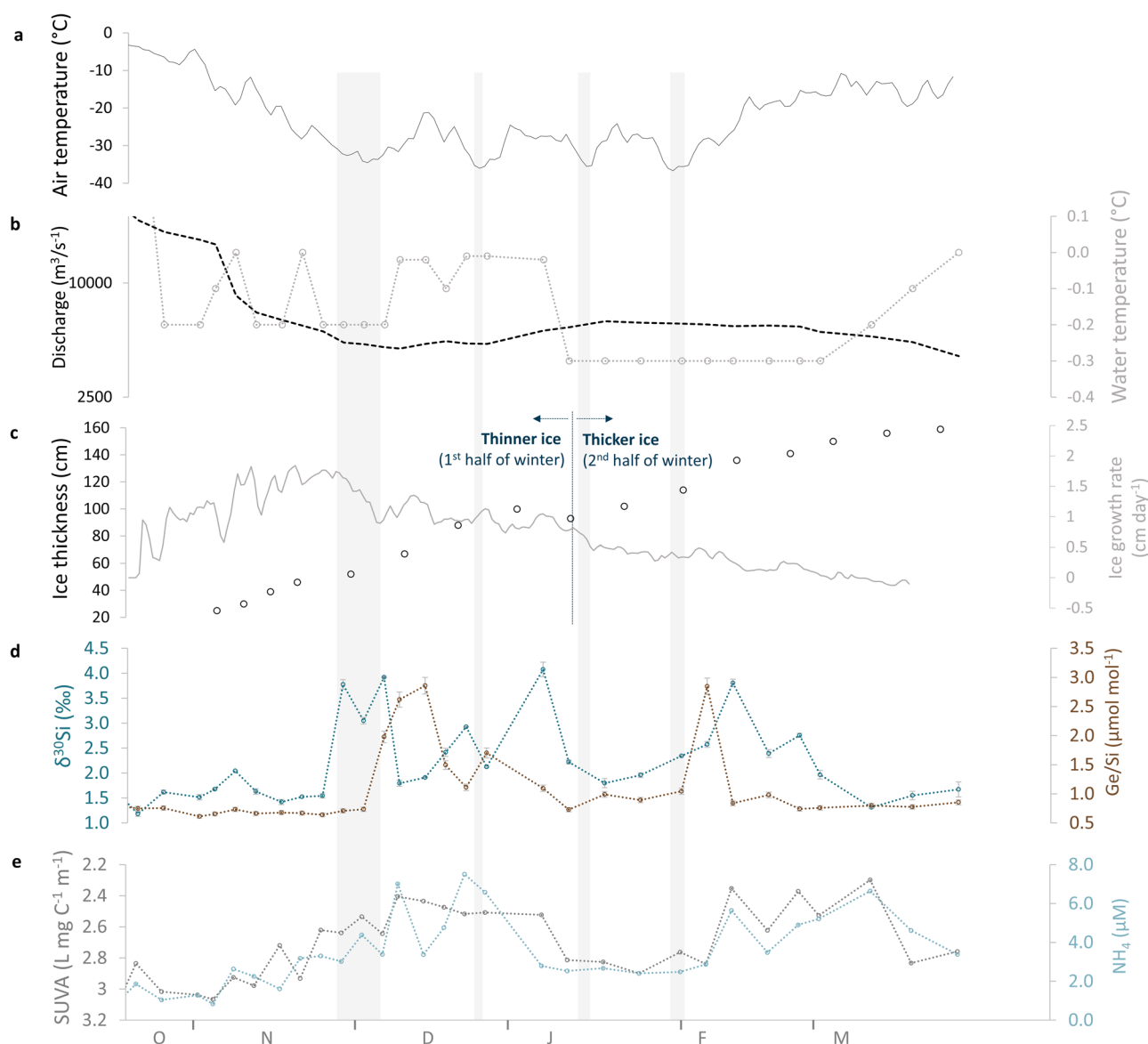


Fig. 3 | Winter chemical monitoring of the Lena River water. Between 15th October 2018 and 31st March 2019 (O, N, D, J, F, M: months from October until March): (a) Air temperature for the whole Lena catchment, with shaded areas for the colder winter phases with air temperature < -30 °C (ERA5-Land⁴¹); (b) Discharge (dashed line; Roshydromet⁴²) and water temperature (dotted line) at Samoylov station¹⁵;

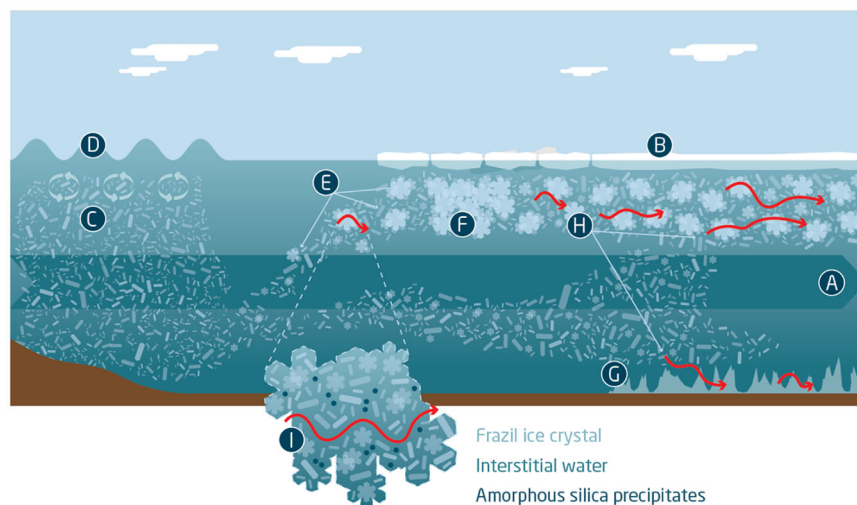
(c) Ice thickness measurement (dots; Roshydromet⁴³) and modeled ice growth rate (full line) at Samoylov station (see Methods); (d) Dissolved Si isotope composition (\pm SD) and Ge/Si ratio (\pm SD) at Samoylov station, (e) SUVA values (Y-axis reverted) and NH₄ concentration at Samoylov station¹⁵.

Fig. 5a, b): this does not trigger sub-ice N and C processing, as reflected by the limited changes in dissolved NH₄ concentration (Supplementary Fig. 5c) or SUVA values (Supplementary Fig. 5d). (ii) One of the two conditions is met in winter 2021–2022 (discharge is high, Supplementary Fig. 5a) or the two conditions are met in winter 2018–2019 (discharge is high, Supplementary Fig. 5a; water temperature < -0.1°C; Supplementary Fig. 5b): this triggers sub-ice N and C processing and induces changes in NH₄ concentrations and SUVA values (Supplementary Fig. 5c, d). Additional support for the importance of a turbulent flow (high winter discharge) to trigger the formation of microzones are the $\delta^{30}\text{Si}$ data reported at the Upper Lena outlet (five river water samples collected at Yakutsk during the winter 2012–2013): no riverine $\delta^{30}\text{Si}$ values heavier than 1.86 ‰ are reported during that winter²⁹ (Supplementary Fig. 6a). This is in line with the low discharge of the winter 2012–2013 relative to the winter 2018–2019 at the Lena outlet (Supplementary Fig. 6b), thereby limiting the potential to trigger amorphous silica precipitation in microzones.

Projected impact of river ice duration decline on sub-ice nutrients processing

In a warming Arctic, river ice duration is expected to decline³. This has already been observed in the Lena catchment with earlier ice break-up and later freeze-up on the Lena River since 1940¹⁵. Since winter provides more than one-third of the dissolved inorganic N input from the Lena to the Arctic Ocean⁶, shortening river ice duration may contribute to the recent annual decline (2003–2019) in inorganic N fluxes observed for the Lena River and for five other major Arctic rivers³⁰. However, a long-term trend of increasing river discharge is observed in the Lena River³¹ and the N supply from permafrost thaw is predicted to increase^{32,33}, likely arousing biogeochemical changes further out in the Arctic Ocean^{34,35}. The organic and inorganic N winter input to the river is expected to spatially differ throughout a catchment or between Arctic river catchments depending on ecosystems, permafrost regimes and changes in discharge³⁶. This leads to more N input to the river from different sources but less time for sub-ice microbial processing of N due to reduced river-ice duration. A far-reaching

Fig. 4 | Processes leading to the formation of microzones in river ice. Longer reaction time for solutes in the water column under river ice cover (red arrows). **A:** Flow; **B:** Stable ice cover; **C:** Frazil produced in supercooled water ($T < 0^\circ\text{C}$); **D:** Turbulent flow entrains frazil in flow; **E:** Frazil agglomerates; **F:** Frazil tends to accumulate at slope transitions; **G:** Frazil sticks to bed matter to form anchor ice; **H:** Microzones with longer reaction time for winter biogeochemical processes in the water column; **I:** Water with longer time in the water column (heavy Si isotope composition, high Ge/Si) and amorphous silica precipitates (light Si isotope composition, low Ge/Si). Graphical design by Y. Nowak.



implication from our findings is that shortening the duration for sub-ice N processing with more organic and inorganic N input may tilt the balance towards the production or consumption of nitrous oxide (N_2O), an intermediate product of denitrification. Ultimately, climate-driven shifts in river discharge and ice cover change spring emissions of N_2O , a greenhouse gas with a global warming potential > 270 times higher than CO_2 at the century time scale, and more generally the extent of Arctic river exchanges with the atmosphere³⁷. In permafrost-dominated river catchments, short-term ice-driven reductions in winter inorganic N flux may be exceeded by longer-term permafrost catchment fluxes.

Methods

Environmental setting

The Lena watershed area ($2.61 \times 10^6 \text{ km}^2$) extends ~ 2400 km from north to south and is underlain by $>70\%$ of continuous permafrost (calculated from ref. 38). The vegetation cover in the catchment is mainly forest (72.1%) and shrubland (12.5%)³⁹. Four major sub-basins can be identified (contribution to annual streamflow by decreasing order²⁰): the Upper Lena (42%), the Aldan (30%), the Lower Lena (19%) and the Vilui (9%) ending by the outlet of the Lena catchment (where the Research Station Samoylov Island is located).

Water sampling and biogeochemical characterization

Water samples were collected from the river surface in the center of the Oleneskaya Channel near Samoylov Island (Latitude 72.368°N ; Longitude 126.4595°E) using a prerinsed HDPE 1 L bottle (in summer) or a UWITEC 1 L water sampler (under ice). Sampling started on 20th April 2018 at a frequency of \sim every four days for almost one year until 28th March 2019. During the open water period (28 May 2018 to 22 October 2018), water was sampled from a small boat, and during the ice-covered period (until 27 May 2018 and from 23 October 2018), via a hole drilled through the river ice. Two samples during the river ice break-up, as well as four samples during the ice freeze-up in October, were taken from the shore due to the inaccessibility of a more centered location on the river channel. Water samples filtered through a $0.45 \mu\text{m}$ cellulose acetate filter (which had been rinsed with 20 ml sample water) were used for Si isotope composition and Ge concentration measurements in this study (see below).

The following biogeochemical parameters were measured on the same water samples¹⁵ and used in this study: the water temperature, the electrical conductivity, the optical index SUVA ($\text{L mg}^{-1} \text{ m}^{-1}$) (calculated by dividing the decadal absorption (A_{254}/l) at 254 nm (m^{-1}), where A_{254} is the absorbance at 254 nm and l the optical path length of the used cuvette in the spectrophotometer, by the dissolved organic carbon concentration (mg L^{-1})) which is correlated with aromaticity and molecular weight of

dissolved organic carbon, the concentration in silicon (Si), and the concentration in ammonium (NH_4). An unfiltered water sample was collected at the same location to measure the oxygen isotope composition ($\delta^{18}\text{O}$). The $\delta^{18}\text{O}$ data in river water collected from Samoylov (Lena monitoring, winter 2018-2019¹⁵) were compared with $\delta^{18}\text{O}$ data in river water collected from Zhigansk, located about 800 km upstream (ArcticGRO, winter 2018-2019⁴⁰) (Supplementary Fig. 2).

Air temperature, discharge and ice thickness measurements

The air temperature at 2 m for 2018-2019 for the Lena catchment, and for the four major sub-basins (Upper Lena, Aldan, Vilui, Lower Lena) were taken from ERA5-Land⁴¹. The discharge data of the Lena River used in this study (2018-2019) are based on the monitoring by the Russian Federal Service for Hydrometeorology and Environmental Monitoring and data available at www.arcticgreatrivers.org (Roshydromet⁴²). The discharge data for Samoylov station were corrected for the distance difference between the gauge station at Kusur (Roshydromet station 3821) and the water sampling station at Samoylov Island (~ 220 km) using a Lena River propagation speed estimate (88 km d^{-1})⁴³. The discharge data for the three major sub-basins (Upper Lena, Aldan, Vilui) are from the three corresponding Roshydromet stations (3042, 3229, and 3329, respectively). The ice thickness measurements were taken from Roshydromet station 3821⁴².

Ice growth rate modelling

Following differential equations⁴⁴, we calculated the daily rate of change of river ice growth of a dynamic two-layer system of snow and ice. Although the equations were originally developed for sea ice, they can be applied to the lake and river ice as well. Since brine entrapment and release are negligible for river ice, we assumed that the freezing point of liquid water below the ice remained at 0°C . Furthermore, we assumed linear temperature gradients and constant thermal conductivities for the snow and ice layers. While the thermal conductivity of gas-free freshwater ice is fixed at $2.2 \text{ W m}^{-1}\text{K}^{-1}$, the thermal conductivity of snow is variable and primarily influenced by snow density. Assuming a slightly compacted snow layer with a density of 322 kg m^{-3} , we used a snow thermal conductivity of $0.3 \text{ W m}^{-1}\text{K}^{-1}$ as a baseline condition⁴⁵. The snow's insulating properties mitigate ice growth and need to be carefully considered in the model. The baseline density (322 kg m^{-3}) falls within the typical range of Arctic snowpack densities⁴⁶ and between the density ranges for settled and wind-packed snow¹⁷. In a recent Arctic sea ice study related to the MOSAiC expedition, Macfarlane et al.⁴⁷ found that the average thermal conductivity of snow ($0.26 \pm 0.05 \text{ W m}^{-1}\text{K}^{-1}$) remains relatively constant over time, regardless of the underlying sea ice type. Hence, the thermal resistance of snow is primarily influenced by its height, which in turn affects the rate of ice growth.

The ice growth rate (dH/dt) is calculated by equation (1), where κ_i is the thermal conductivity of ice, κ_s is the thermal conductivity of snow, T_f is the freezing point of water, T_s is the snow surface temperature, H is the ice thickness, h is the snow thickness, L_f is the latent heat of fusion of water ($334\,000\text{ J kg}^{-1}$), and ρ_i is the density of ice (917 kg m^{-3}). In equation (1), we used daily mean air temperatures for T_s (ERA5-Land⁴¹) and assumed that they approximate the snow surface temperature. For h , we used daily measurements of snow height (ERA5-Land⁴¹). We then calculated the ice thickness with equation (2) and applied a daily time step for the ice growth rate.

We calibrated the river ice growth model by multiplying the daily snow depth by a factor, alpha, to match the modelled output with the maximum observed river ice thickness. With an alpha = 0.22, the R^2 between the predicted values and the ice thickness observations ($n = 21$) for a linear fit is 0.978. We present an envelope of ice growth trends between an alpha of 0.01 (no snow) to 1.0 (raw snow depth data from the Lena catchment observatory). For an alpha of 0.22, we carried out another sensitivity analysis by varying the snow thermal conductivity between 0.21 and $0.46\text{ W m}^{-1}\text{K}^{-1}$ (Supplementary Fig. 7). The minimum and maximum thermal conductivities are associated with the minimum and maximum snow densities¹⁷ reported for the islands of Samoylov in April 2016 and 2017. Our sensitivity analysis shows that varying the snow thermal conductivity from 0.21 to $0.46\text{ W m}^{-1}\text{K}^{-1}$ has minimal impact on ice growth compared to variations in snow height.

$$\frac{dH}{dt} = \frac{\kappa_i(T_f - T_s)}{L_f \rho_i \left[H + \left(\frac{\kappa_i}{\kappa_s} \right) h \right]} \quad (1)$$

$$H(t) = \frac{dH}{dt}(t) \times 3600 \times 24 + H(t - 1) \quad (2)$$

Water silicon isotope analysis

Silicon isotope compositions were determined on all water samples from the Lena River ($n = 72$). The dissolved organic carbon was removed from the sample matrix by reflux⁴⁸ with concentrated HNO_3 and H_2O_2 . The Si was separated from the matrix with a two-stages column chemistry procedure using an anion exchange resin (Bio-Rad AG MP-1) followed by a cation exchange resin (Bio-Rad AG50W-X12)⁴⁹. The Si recoveries were > 95% and Na^+ , SO_4^{2-} and Cl^- concentrations were below the detection limit following column chemistry. The combined procedural Si blank for organic carbon removal and column chemistry was below $0.36\text{ }\mu\text{M}$.

The silicon isotope composition ($\delta^{30}\text{Si}$) was analyzed by MC-ICP-MS (Neptune Plus™ High-Resolution Multicollector ICP-MS, Thermo Fisher Scientific, Earth & Life Institute, UCLouvain, Belgium) in wet plasma mode in medium resolution ($\Delta m/m \sim 6000$) using a PFA nebulizer of $100\text{ }\mu\text{l min}^{-1}$ uptake rate. The instrumental mass bias was corrected using the standard-sample bracketing technique and an external Mg doping⁵⁰. The analyses were performed in 2% HNO_3 matrix, with a typical sensitivity of 7 V for 0.07 mM Si and an instrumental blank < 30 mV. The $\delta^{30}\text{Si}$ compositions are expressed in relative deviations of $^{30}\text{Si}/^{28}\text{Si}$ ratio from the NBS-28 reference standard using the common δ -notation (‰) as follows: $\delta^{30}\text{Si} = \left[\frac{(^{30}\text{Si}/^{28}\text{Si})_{\text{sample}}}{(^{30}\text{Si}/^{28}\text{Si})_{\text{NBS-28}}} - 1 \right] \times 1000$. One measurement comprises 30 cycles with 4.2 s integration time corrected by blank in a 2% HNO_3 matrix. Each single δ -value represents one sample run and two bracketing standards. The $\delta^{30}\text{Si}$ values are reported as the mean of isotopic analyses from multiple analytical sessions at least in duplicate. The $\delta^{30}\text{Si}$ and $\delta^{29}\text{Si}$ measurements fit within error onto the theoretical mass-dependent fractionation array supporting the interference-free determination of all three Si isotopes via MC-ICP-MS. The long-term precision and accuracy of the MC-ICP-MS $\delta^{30}\text{Si}$ values were assessed from multiple measurements within each analytical session on reference materials: the values obtained for Diatomite ($\delta^{30}\text{Si} = 1.31 \pm 0.08\text{ ‰}$, SD, $n = 21$) and Quartz Merck ($\delta^{30}\text{Si} = -0.01 \pm 0.08\text{ ‰}$, SD, $n = 8$) are consistent with previously reported

values for these standards (Diatomite: $\delta^{30}\text{Si} = 1.26 \pm 0.10\text{ ‰}$ ⁵¹; Quartz Merck: $\delta^{30}\text{Si} = -0.01 \pm 0.12\text{ ‰}$ ⁵²).

Water Ge concentration analysis

The Ge concentration in all water samples from the Lena River ($n = 72$) was determined by ICP-mass spectrometry (ICP-MS, ICAPQ Thermo Fisher Scientific, Earth & Life Institute, UCLouvain, Belgium)⁴⁹ with a PFA nebulizer of $400\text{ }\mu\text{l min}^{-1}$ uptake rate, a quartz cyclonic spray chamber, and in 2% HNO_3 . The three isotopes ^{72}Ge , ^{73}Ge and ^{74}Ge were monitored during Ge concentration analyses, and the most abundant isotope ^{74}Ge , was used for the measurement given the higher sensitivity and the lower detection limit compared to other isotopes. Rhodium was used as an internal standard to correct for instrumental drift. The typical ^{74}Ge sensitivity was 22,000 cps per $\mu\text{g l}^{-1}$ and ^{103}Rh sensitivity was 100,000 cps per $\mu\text{g l}^{-1}$. Accuracy and long-term repeatability of the analysis were assessed by measuring two international riverine standards, namely SLRS-5 ($[\text{Ge}] = 0.083 \pm 0.014\text{ nM}$, SD; $n = 3$) and SLRS-6 ($[\text{Ge}] = 0.097 \pm 0.007\text{ nM}$, SD; $n = 3$) in line with the published values (SLRS-5: $0.151 \pm 0.151\text{ nM}$ ⁵³, $n = 34$; SLRS-6: $0.138 \pm 0.096\text{ nM}$ ⁵⁴, $n = 45$). The detection limit for Ge is 0.04 nM and the analytical precision of the measurement is $\pm 8\%$ for Ge concentrations < 0.013 nM and $\pm 4\%$ for Ge concentrations > 0.013 nM. The standard deviation of our Ge/Si ratio determinations is 10%.

Isotope mass balance calculation

Following an isotope mass balance, the measured Si isotope composition of the water at Samoylov station during the ice-covered period ($\delta^{30}\text{Si}_{\text{river water ice-covered period}}$) is a mixing between a proportion x of river discharge from the water column with an average Si isotope composition from the open water period ($\delta^{30}\text{Si}_{\text{river water open-period}} = 1.50 \pm 0.28\text{ ‰}$) and a proportion $(1-x)$ of river discharge from microzones with a Si isotope composition dictated by the fractionation factor of amorphous silica precipitation of $+5\text{ ‰}$ ¹¹ relative to $\delta^{30}\text{Si}_{\text{river water open-period}}$ ($\delta^{30}\text{Si}_{\text{microzones}} = 6.5\text{ ‰}$) (equation (3)).

$$\delta^{30}\text{Si}_{\text{river water ice-covered period}} = x * \delta^{30}\text{Si}_{\text{river water open-period}} + (1 - x) * \delta^{30}\text{Si}_{\text{microzone}} \quad (3)$$

For each Si isotope measurement at Samoylov station, the proportion $(1-x)$ of river discharge from the microzones was calculated during the ice-covered period (Supplementary Fig. 4). The two following assumptions were made when using the isotope mass balance model: (i) the fractionation factor reflects a unidirectional kinetic isotope effect during the fast precipitation of solids and has been considered as constant¹¹. This is a reasonable assumption within the range of Al concentration in the Lena River (between 0 and $0.4\text{ }\mu\text{M}$ during the winter¹⁵), which likely follows an increase in concentration in microzones similar to Si (by a factor of 8 minimum, corresponding to minimum $\sim 3\text{ }\mu\text{M Al}$); (ii) the $\delta^{30}\text{Si}_{\text{river water open-period}}$ is an average with a range of variability of 0.28 ‰ reflecting the processes occurring prior to the winter period. The range of variability of 0.28 ‰ is reflected in the uncertainty on the calculated proportion of river discharge flowing through microzones during the winter.

Data availability

All data are directly available from PANGAEA (10.1594/PANGAEA.913197).

Received: 13 June 2024; Accepted: 6 November 2024;

Published online: 25 November 2024

References

- Rantanen, M. et al. The Arctic has warmed nearly four times faster than the globe since 1979. *Commun. Earth Environ.* **3**, 1–10 (2022).
- Park, H. et al. Quantification of warming climate-induced changes in terrestrial Arctic River ice thickness and phenology. *J. Climate* **29**, 1733–1754 (2016).

3. Parmesan, C. et al. Terrestrial and freshwater ecosystems and their services, in: *Climate Change 2022: Impacts, Adaptation and Vulnerability, Contribution of Working Group II to the Sixth Assessment Report of the Intergovernmental Panel on Climate Change*. Cambridge University Press, Cambridge, UK and New York, NY, USA, pp. 197–377 (2022).
4. Sanders, T. et al. Seasonal nitrogen fluxes of the Lena River Delta. *Ambio* **51**, 423–438 (2022).
5. Knights, D., Piliouras, A., Schwenk, J., Hariharan, J. & Russoniello, C. Seasonal and morphological controls on nitrate retention in Arctic Deltas. *Geophys. Res. Lett.* **50**, e2022GL102201 (2023).
6. Holmes, R. et al. Seasonal and annual fluxes of nutrients and organic matter from large rivers to the Arctic Ocean and surrounding seas. *Estuar. Coast.* **35**, 369–382 (2012).
7. Butler, T. M. et al. Microbial community dynamics during lake ice freezing. *Sci. Rep.* **9**, 6231 (2019).
8. Alonso-Sáez, L. et al. Winter bloom of a rare betaproteobacterium in the Arctic Ocean. *Front. Microbiol.* **5**, 425 (2014).
9. Lannuzel, D. et al. The future of Arctic sea-ice biogeochemistry and ice-associated ecosystems. *Nat. Clim. Chang.* **10**, 983–992 (2020).
10. Dietzel, M. Impact of cyclic freezing on precipitation of silica in Me–SiO₂–H₂O systems and geochemical implications for cryosols and -sediments. *Chem. Geol.* **216**, 79–88 (2005).
11. Oelze, M., von Blanckenburg, F., Bouchez, J., Hoellen, D. & Dietzel, M. The effect of Al on Si isotope fractionation investigated by silica precipitation experiments. *Chem. Geol.* **397**, 94–105 (2015).
12. Hirst, C. et al. Silicon isotopes reveal a non-glacial source of silicon to Crescent Stream, McMurdo Dry Valleys, Antarctica. *Front. Earth Sci.* **8**, 229 (2020).
13. Hirst, C. et al. Evidence for late winter biogeochemical connectivity in permafrost soils. *Commun. Earth Environ.* **4**, 1–10 (2023).
14. Fernandez, N. M., Perez-Fodich, A., Dery, L. A. & Druhan, J. L. A first look at Ge/Si partitioning during amorphous silica precipitation: Implications for Ge/Si as a tracer of fluid-silicate interactions. *Geochim. Cosmochim. Acta* **297**, 158–178 (2021).
15. Juhls, B. et al. Identifying drivers of seasonality in Lena River biogeochemistry and dissolved organic matter fluxes. *Front. Environ. Sci.* **8**, 53 (2020).
16. Barrette, P. D. Understanding frazil ice: The contribution of laboratory studies. *Cold Reg. Sci. Tech.* **189**, 103334 (2021).
17. Lütjen, M. et al. Drivers of winter ice formation on Arctic water bodies in the Lena Delta, Siberia. *Arct. Antarct. Alp. Res.*, accepted (2024).
18. Beltaos, S. et al. River ice formation. Committee on River Ice Processes and the Environment, Canadian Geophysical Union Hydrology Section, Edmonton, Alberta, Canada, ISBN 978-0-9920022-0-6 (2013).
19. Hoyt, W. G. The effect of ice on streamflow. USGS, Washington Government printing Office Water Supply paper (1913).
20. Ye, B., Yang, D. & Kane, D. L. Changes in Lena River streamflow hydrology: Human impacts versus natural variations. *Water Resour. Res.* **39**, 1200 (2003).
21. White, K. Determining the intrinsic permeability of frazil ice. Part 1. *Lab. Invest.* **21**, (1991).
22. Osterkamp, T. E., Gilfillan, R. E. & Benson, C. S. Observations of stage, discharge, pH, and electrical Conductivity during periods of ice formation in a small subarctic stream. *Water Resour. Res.* **11**, 268–272 (1975).
23. Gurevich, E. V. Influence of air temperature on the river runoff in winter (the Aldan river catchment case study). *Russ. Meteorol. Hydrol.* **34**, 628–633 (2009).
24. Briggs, M. A., Day-Lewis, F. D., Zarnetske, J. P. & Harvey, J. W. A physical explanation for the development of redox microzones in hyporheic flow. *Geophys. Res. Letters* **42**, 4402–4410 (2015).
25. Kellogg, C. T. E., McClelland, J. W., Dunton, K. H. & Crump, B. C. Strong seasonality in Arctic estuarine microbial food webs. *Front. Microbiol.* **10**, 2628 (2019).
26. Papale, M. et al. Benthic microbial communities in a seasonally ice-covered sub-Arctic River (Pasvik River, Norway) are shaped by site-specific environmental conditions. *Microorganisms* **10**, 1022 (2022).
27. Nyantekyi-Kwakye, B., Ahmed, T., Clark, S. P., Tachie, M. F. & Dow, K. Effect of discharge and upstream jam angle on the flow distribution beneath a simulated ice jam. *Can. J. Civ. Eng.* **46**, 413–423 (2019).
28. Juhls, B. et al. Lena River surface water monitoring near the Samoylov Island Research Station [dataset publication series]. PANGAEA, <https://doi.org/10.1594/PANGAEA.913197> (2020).
29. Sun, X. et al. Stable silicon isotopic compositions of the Lena River and its tributaries: Implications for silicon delivery to the Arctic Ocean. *Geochim. Cosmochim. Acta* **241**, 120–133 (2018).
30. Tank, S. E. et al. Recent trends in the chemistry of major northern rivers signal widespread Arctic change. *Nat. Geosci.* **16**, 789–796 (2023).
31. Tananaev, N. I., Makarieva, O. M. & Lebedeva, L. S. Trends in annual and extreme flows in the Lena River basin, Northern Eurasia. *Geophys. Res. Letters* **43**, 10,764–10,772 (2016).
32. Zhang, S.-M. et al. Export of nutrients and suspended solids from major Arctic rivers and their response to permafrost degradation. *Adv. Clim. Change Res.* **12**, 466–474 (2021).
33. Strauss, J. et al. A globally relevant stock of soil nitrogen in the Yedoma permafrost domain. *Nat. Commun.* **13**, 6074 (2022).
34. Terhaar, J., Lauerwald, R., Regnier, P., Gruber, N. & Bopp, L. Around one third of current Arctic Ocean primary production sustained by rivers and coastal erosion. *Nat. Commun.* **12**, 169 (2021).
35. Debyser, M. C. F. et al. The importance of riverine nutrient supply for the marine silica pump of Arctic Shelves: Evidence from the Laptev Sea. *Glob. Biogeochem. Cycles* **38**, e2023GB007828 (2024).
36. Feng, D. et al. Recent changes to Arctic river discharge. *Nat. Commun.* **12**, 6917 (2021).
37. Allen, G. H. & Pavelsky, T. M. Global extent of rivers and streams. *Science* **361**, 585–588 (2018).
38. Obu, J. et al. Northern Hemisphere permafrost map based on TTOP modelling for 2000–2016 at 1km² scale. *Earth-Sci. Rev.* **193**, 299–316 (2019).
39. Amon, R. M. W. et al. Dissolved organic matter sources in large Arctic rivers. *Geochim. Cosmochim. Acta* **94**, 217–237 (2012).
40. Holmes, R. M., McClelland, J. W., Tank, S. E., Spencer, R. G. M. & Shiklomanov, A. I. Arctic Great Rivers Observatory. Water Quality Dataset, Version 2022-09–10 (2021).
41. Muñoz Sabater, J. ERA5-Land hourly data from 1950 to present. Copernicus Climate Change Service (C3S) Climate Data Store (CDS) (2019).
42. Shiklomanov, A. I., Holmes, R. M., McClelland, J. W., Tank, S. E., & Spencer, R. G. M. ArcticGRO Discharge Dataset, Version 2020-01-23. Arct. Gt. Rivers Obs. Discharge (2018).
43. Smith, L. C. & Pavelsky, T. M. Estimation of river discharge, propagation speed, and hydraulic geometry from space: Lena River, Siberia. *Water Resour. Res.* **44**, W03427 (2008).
44. Leppäranta, M. A review of analytical models of sea-ice growth. *Atm.-Ocean* **31**, 123–138 (1993).
45. Goodrich, L. E. The influence of snow cover on the ground thermal regime. *Can. Geotech. J.* **19**, 421–432 (1982).
46. Ashton, G. D. River and lake ice thickening, thinning, and snow ice formation. *Cold Reg. Sci. Technol.* **68**, 3–19 (2011).
47. Macfarlane, A. R. et al. Temporospatial variability of snow's thermal conductivity on Arctic sea ice. *The Cryosphere* **17**, 5417–5434 (2023).
48. Hughes, H. J. et al. Controlling the mass bias introduced by anionic and organic matrices in silicon isotopic measurements by MC-ICP-MS. *J. Anal. At. Spectrom.* **26**, 1892–1896 (2011).
49. Gaspard, F. et al. Imprint of chemical weathering and hydrothermalism on the Ge/Si ratio and Si isotope composition of

- rivers in a volcanic tropical island, Basse-Terre, Guadeloupe (French West Indies). *Chem. Geol.* **577**, 120283 (2021).
50. Cardinal, D., Alleman, L. Y., Jong, J., de, Ziegler, K. & André, L. Isotopic composition of silicon measured by multicollector plasma source mass spectrometry in dry plasma mode. *J. Anal. At. Spectrom.* **18**, 213–218 (2003).
51. Reynolds, B. C. et al. An inter-laboratory comparison of Si isotope reference materials. *J. Anal. At. Spectrom.* **22**, 561–568 (2007).
52. Abraham, K. et al. $\delta^{30}\text{Si}$ and $\delta^{29}\text{Si}$ Determinations on USGS BHVO–1 and BHVO-2 reference materials with a new configuration on a Nu Plasma Multi-Collector ICP-MS. *Geostand. Geoanal. Res.* **32**, 193–202 (2008).
53. Yeghicheyan, D. et al. A compilation of silicon, Rare Earth Element and twenty-One other trace element concentrations in the natural River Water Reference Material SLRS-5 (NRC-CNRC). *Geostand. Geoanal. Res.* **37**, 449–467 (2013).
54. Yeghicheyan, D. et al. A new interlaboratory characterisation of silicon, Rare Earth Elements and twenty-Two other trace element concentrations in the natural River Water Certified Reference Material SLRS-6 (NRC-CNRC). *Geostand. Geoanal. Res.* **43**, 475–496 (2019).

Acknowledgements

The authors benefited from discussions with M. Thomas, M. Villani, E. du Bois d'Aische, C. Osy, P. Roux, L. Lebedeva and T. Sanders. The authors thank the analytical platform MOCA at UCLouvain, M. Brzezinski from University of California Santa Barbara for providing the Diatomite reference material for Si isotope analysis, Y. Nowak for graphical design, the Russian-German Lena Expedition and Research Station Samoylov Island for supporting the Lena River Water Monitoring from 2018 to 2022 and especially S. Volkov and A. Astapov for water sampling. BJ was funded by the BNP Paribas Foundation Climate & Biodiversity Initiative (project FLO CHAR). This study was funded by the European Research Council (ERC) under the European Union's Horizon 2020 research and innovation programme (ERC Starting Grant, WeThaw, grant agreement n°714617), by the Fonds National de la Recherche Scientifique (FNRS, FC69480 and CDR-MOIST), and by the Belgian Science Policy (BELSPO IMPULS, RT/23/LIFTHAW) to S.O.

Author contributions

S.O. designed the study. P.P.O., A.M. and B. J. set up the Lena River monitoring program to collect the water samples. F.G. collected the Si isotope data, and L.M. the Ge concentration data. C.H. shared her expertise about the Lena River catchment and the functioning of large Arctic rivers.

M.A. modeled the growth rate of the river ice over the winter. P.P.O. and B.J. shared their expertise about the annual variability in the riverine chemistry. S.O. wrote the manuscript with contributions from all authors.

Competing interests

The authors declare no competing interests.

Additional information

Supplementary information The online version contains supplementary material available at <https://doi.org/10.1038/s43247-024-01884-9>.

Correspondence and requests for materials should be addressed to Sophie Opfergelt.

Peer review information *Communications Earth & Environment* thanks Kristin Doering, Joanna Carey and the other, anonymous, reviewer(s) for their contribution to the peer review of this work. Primary Handling Editors: Alice Drinkwater and Somaparna Ghosh. [A peer review file is available.]

Reprints and permissions information is available at <http://www.nature.com/reprints>

Publisher's note Springer Nature remains neutral with regard to jurisdictional claims in published maps and institutional affiliations.

Open Access This article is licensed under a Creative Commons Attribution-NonCommercial-NoDerivatives 4.0 International License, which permits any non-commercial use, sharing, distribution and reproduction in any medium or format, as long as you give appropriate credit to the original author(s) and the source, provide a link to the Creative Commons licence, and indicate if you modified the licensed material. You do not have permission under this licence to share adapted material derived from this article or parts of it. The images or other third party material in this article are included in the article's Creative Commons licence, unless indicated otherwise in a credit line to the material. If material is not included in the article's Creative Commons licence and your intended use is not permitted by statutory regulation or exceeds the permitted use, you will need to obtain permission directly from the copyright holder. To view a copy of this licence, visit <http://creativecommons.org/licenses/by-nc-nd/4.0/>.

© The Author(s) 2024